Size-Controlled Synthesis of Magnetite (Fe_3O_4) Nanoparticles Coated with Glucose and Gluconic Acid from a Single Fe(III) Precursor by a Sucrose Bifunctional Hydrothermal Method

Xiaohong Sun, Chunming Zheng, Fuxiang Zhang, Yali Yang, Guangjun Wu, Aimin Yu, and Naijia Guan*

Key Lab of Functional Polymer Materials, Department of Materials Chemistry, College of Chemistry, Nankai University, Tianjin 300071, People's Republic of China

Received: April 27, 2009; Revised Manuscript Received: June 15, 2009

Size-controlled and coated magnetite nanoparticles with glucose and gluconic acid have been successfully synthesized via a simple and facile hydrothermal reduction route using a single iron precursor, $FeCl_3$, and a combination of the inherent chemical reduction capability of sucrose decomposition products and their inorganic coordinating ability. The particle size can be easily controlled in the range of 4−16 nm. Results obtained with and without the addition of sucrose indicate that sucrose is required for the formation of nanoscale and coated magnetite instead of the much larger hematite. Mass spectrometry, Fourier transform infrared spectroscopy, X-ray photoelectron spectroscopy, and thermogravimetry analysis were used to investigate the formation mechanism of the coated nanomagnetite from the single Fe(III) precursor in sucrose. Sucrose acts as a bifunctional agent: (i) it decomposes into reducing species, causing partial reduction of the Fe^{3+} ions to Fe^{2+} ions as required for the formation of Fe_3O_4 and (ii) acts as the source of a capping agent to adjust the surface properties and enable the formation of nanoscale particles. The saturation magnetization of the as-obtained magnetite is measured and greatly related to the particle size.

Introduction

The development of nanometer sized particles has been intensively pursued because of their interesting electrical, optical, magnetic, and chemical properties, which cannot be achieved for their bulk counterparts.[1,2] Magnetic iron oxide nanoparticles containing magnetite (Fe_3O_4) have been widely studied due to their current and promising applications in catalysis,[3] ferrofluids,[4] magnetic storage,[5] magnetic resonance imaging (MRI),[6] separation,[7,8] target-drug delivery,[9] clinical diagnosis,[10−12] etc. Various chemical synthetic routes have been employed to produce magnetite nanoparticles with desired physical and chemical properties, such as coprecipitation of aqueous ferrous (Fe^{2+}) and ferric (Fe^{3+}) salt solution by the addition of a base,[13] microemulsion technique,[14] hydrothermal synthesis,[15] sonochemical approach,[16] nonaqueous route,[17] and thermal decomposition of an organic iron precursor, including $FeCup_3$ (cup = *N*-nitrosophenylhydroxylamine, $C_6H_5N(NO)O^-$),[18] $Fe(CO)_5$,[19] or $Fe(acac)_3$ ($Fe(CH_3COCHCOCH_3)_3$),[20] at high temperature with good size and morphology control.

In the above synthesis routes for nanomagnetite, one challenge was to maintain the coexistence of Fe^{2+} ions and Fe^{3+} ions with a fixed proportion (1:2) in the Fe_3O_4 structure and prevent them from being reoxidized during the experimental processes. Purgation or protection with nitrogen[13,20] or argon[18,19] has been widely used and proved to be feasible. However, the purgation or protection procedure is relatively complicated and expensive for industrial-scale production. Therefore, it is useful to explore and design simple ways to keep the preparation from purgation or protection processes.

The successful applications of the magnetite nanoparticles strongly depend on the tightly controlled particle size and well-defined surface properties. The size and size distribution of the nanoparticles is one of the key parameters that determine the magnetic properties of the particles (ferromagnetic or superparamagnetic with different saturation magnetization).[21] Different methods have been developed to synthesize the magnetite nanoparticles with a controlled size, such as the seed-mediated growth method,[22] varying the surfactant or micelle concentration,[23] or adjusting the pH value or reaction time.[24] Magnetic nanoparticles tend to aggregate due to strong magnetic dipole−dipole attractions between particles combined with van der Waals interparticle attractions and their inherently large surface energy (>100 dyn cm^{-1}).[25] Therefore, coating agents, such as surfactants or capping ligands with some specific functional groups, have been used to modify these particles to prevent the sedimentation and obtain better surface properties. Recently, Kim et al.[26] successfully exchanged dendron ligands onto the surface of high-quality Fe_3O_4 nanocrystals by introducing a new bonding group, hydroxamic acid, to the dendron ligands. Li and co-workers[27] developed a one-pot template-free method for the preparation of amine-functionalized magnetite nanoparticles and hollow nanospheres. Yin et al.[28] synthesized highly water-soluble magnetite colloidal nanocrystals by using a polyelectrolyte, poly(acrylic acid), as the capping agent. Because most of the employed coating agents have environmental concerns and limit the biomedical applications or are expensive for industrial-scale preparation, it is still a challenge to economically synthesize nanoscale magnetite that is bioapplicable.

In this paper, facile and environmentally friendly sucrose and a readily available Fe(III) precursor, $FeCl_3$, were used to synthesize the coated and size-controlled nanomagnetite without either a purgation or a protection procedure. The size of the

* To whom correspondence should be addressed. E-mail: guannj@nankai.edu.cn. Phone: +86-022-23509140.

10.1021/jp9038682 CCC: $40.75
Published on Web 08/18/2009

magnetite nanoparticles could be controlled easily from 4 to 16 nm by adjusting the sucrose concentration. The mechanism for the formation of coated and nanoscale Fe_3O_4 from the single iron precursor, $FeCl_3$, in sucrose was studied in detail by mass spectrometry (MS), infrared (IR), X-ray photoelectron spectroscopy (XPS), and thermogravimetry (TG) analysis. The saturation magnetization (*M*s) of the as-obtained magnetite is greatly related to the particle size.

Experimental Section

Materials. The chemical reagents used in this work are ferric chloride ($FeCl_3$), sucrose, and ammonia solution ($NH_3 \cdot H_2O$, 25%). All the chemical reagents are of analytical grade.

Synthesis of Magnetite (Fe_3O_4) Nanoparticles in Sucrose. In a typical experimental procedure, 3.33 g of sucrose was dissolved in 50 mL of deionized water and then 0.9 g of $FeCl_3$ was added with vigorous stirring. The molar ratio of sucrose to $FeCl_3$ is 7:4 (sample a). The pH value of the solution was adjusted to ca. 10 by the dropwise addition of 25% ammonia solution. Vigorous stirring was carried on for about 30 min, and the obtained mixture was then transferred into a Teflon-lined stainless steel autoclave (25 mL capacity) for crystallization at 180 °C for 48 h. After the reaction system was naturally cooled to room temperature, the product was isolated from the liquid phase by centrifugation and then thoroughly washed three times with deionized water to remove water-soluble organic byproducts. The final product was dried at 60 °C overnight and appeared as a fine black-brown powder. The process was repeated with variation of the molar ratio of sucrose to $FeCl_3$ to 7:8 (sample b) and 7:16 (sample c). Moreover, when the sucrose concentration was decreased further, no pure phase magnetite nanoparticles larger than 16 nm in average diameter could be synthesized. It is important to note that a control experiment without the addition of sucrose led to the formation of hematite (α-Fe_2O_3) instead of magnetite (Fe_3O_4) using the same reaction procedure as described above.

Characterization. Standard and high-resolution transmission electron microscopy (TEM and HRTEM) measurements were performed on a Philips Tecnai F20 microscope. All samples subjected to TEM measurements were ultrasonically dispersed in alcohol and drop-cast onto copper grids. X-ray powder diffraction (XRD) patterns of the samples were performed at room temperature on a Rigaku D/max 2500 diffractometer with a graphite monochromator and Cu Kα radiation ($\lambda = 0.154$ nm). Typically, the data were collected from 10° to 80° with a resolution of 0.2°. The average crystallite size was estimated using the Debye−Scherrer equation, $D = K\lambda/(\beta \cos \theta)$, where D is the average crystal diameter, β is the corrected peak width (full width at half-maximum), K is a constant related to the shape of the crystallites ($K = 0.94$), λ is the wavelength of the X-rays employed, and θ is the diffraction angle. The width of the diffraction peak with the highest intensity was selected for the calculation. Raman spectra were measured by a Renishaw inVia Raman microscope at room temperature with the 514 nm line of an Ar ion laser as an excitation source. Mass spectrometry (MS) was carried out on a FINNIGAN LCQ-Advantage mass spectrometer under the following conditions: ionizing voltage, 28 eV; ionizing current, 300 μA; ion source temperature, 250 °C. Fourier transform infrared (FT-IR) spectra were recorded on a Bruker Vector 22 FT-IR spectrophotometer using a KBr pellet. The X-ray photoelectron spectroscopy (XPS) measurements were acquired using a PHI 5300 ESCA XPS spectrometer with monochromatic Mg KR excitation. Thermogravimetry analysis (TGA) was performed using a Rigaku thermogravimetry-differential thermal analysis (TG-DTA) analyzer with a heating rate of 6 °C/min in nitrogen. Magnetization studies were performed at room temperature using a LDJ 9600 VSM magnetometer.

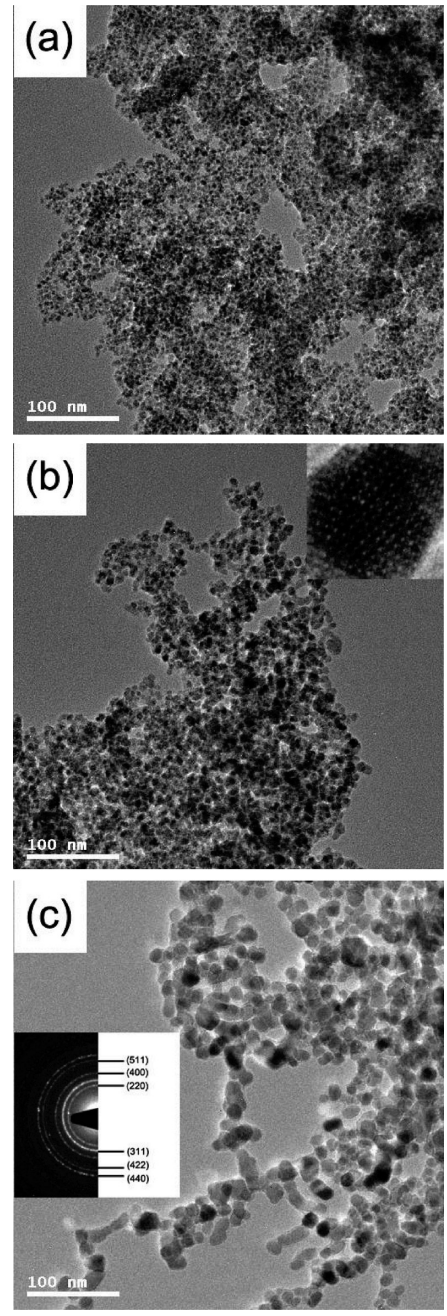

Figure 1. TEM images of the Fe_3O_4 nanoparticles prepared with various sucrose concentrations. The molar ratio of sucrose to $FeCl_3$ was 7:4 (sample a), 7:8 (sample b), and 7:16 (sample c). (b, inset) HRTEM image of sample b. (c, inset) ED of sample c.

Results and Discussion

Structural Characterization. Figure 1 shows the TEM images of all the Fe_3O_4 nanoparticles prepared by varying the sucrose concentration. All the samples show the nearly uniform distribution of particle size (high-magnification TEM images can be found in the Supporting Information). When the size of at least 50 particles from the TEM images is measured, the particle size is about 4, 8, and 16 nm, respectively, for samples a, b, and c, which compares well with the average crystallite

TABLE 1: Average Grain Size and Crystallite Size of Magnetite Nanoparticles Prepared by Varying the Sucrose Concentration

samples	molar ratios of sucrose to $FeCl_3$	grain size from TEM (nm)	crystallite size from XRD (nm)
a	7:4	4 ± 0.6	4.2
b	7:8	8 ± 1.8	8.7
c	7:16	16 ± 2.4	17.1

size determined by Debye−Scherrer analysis of the X-ray diffraction data for the three different samples (Table 1). It clearly indicates that there is a continuous increase of particle size upon decreasing the sucrose concentration, which is because sucrose, as the dextran, acts as an inhibitor of the growth of the particles.[29] The relative standard deviation values suggest that the magnetite nanoparticles prepared at high sucrose concentration are relatively more monodispersed than the particles prepared at low sucrose concentration. High-resolution TEM (inserted in Figure 1b) of sample b shows well-defined lattice planes with perfect crystallinity. The planes have an interplanar distance of 0.48 nm, which is characteristic of (111) spinel planes and often observed for magnetite particles.[30] The electron diffraction (ED) pattern of the selected portion of sample c, inserted in Figure 1c, presents clear and well-defined rings that can be indexed to the magnetite structure. The reflections characteristic of other iron oxides are not observed.

The XRD pattern was used to identify the iron oxide phases of all the samples in Figure 2 obtained by decreasing the sucrose concentration. All the peak positions at 18.2 (111), 30.1 (200), 35.4 (311), 43.0 (400), 53.7 (422), 57.2 (511), and 62.6 (440) are consistent with the standard X-ray data for the magnetite phase (JCPDS no. 19-0629). There is a continuous broadening of each peak with the increase in sucrose concentration, which, as described above, is attributed to the decrease in the particle size and verified quantitatively by using Scherrer's equation. The particle sizes measured by Scherrer's equation are quite close to the TEM result (see Table 1). It means that all the as-synthesized particles are single crystals. On the other hand, the relative XRD peak intensities decrease with increasing sucrose concentration, which indicates that the relative crystallinity of the magnetite decreased. Besides magnetite peaks, we did not observe any other iron oxide peaks in the diffraction pattern for any of the samples.

Because the XRD patterns of magnetite (Fe_3O_4) and maghemite (γ-Fe_2O_3) are very similar,[31] Raman spectroscopy was used to distinguish the different structural phases of iron oxides. Magnetite has a main band centered at 668 cm^{-1} (A_{1g}), whereas maghemite shows broad peaks around 720, 500, and 350 cm^{-1}.[32] Figure 3 illustrates the Raman spectroscopy measured for sample c. It shows the main feature at 667 cm^{-1}, characteristic of magnetite. No other characteristic iron oxide bands, such as those for maghemite (γ-Fe_2O_3) or hematite (α-Fe_2O_3), were observed. This further proves that the phase of the iron oxide is magnetite.

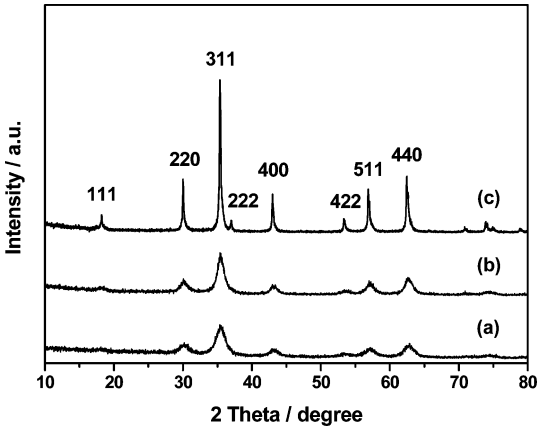

Figure 2. XRD of Fe_3O_4 samples prepared with various sucrose concentrations. The molar ratio of sucrose to $FeCl_3$ was 7:4 (sample a), 7:8 (sample b), and 7:16 (sample c).

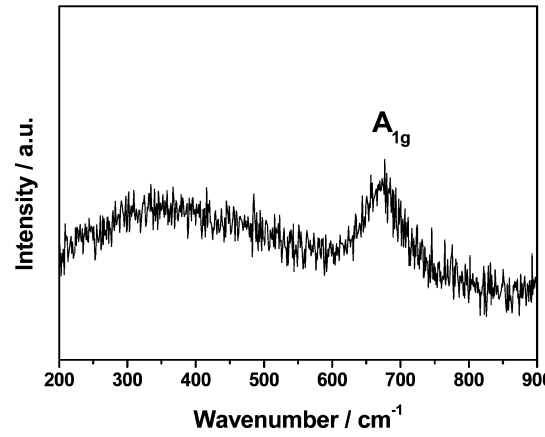

Figure 3. Raman spectroscopy of magnetite sample c.

Reduction and Coating Mechanism for the Formation of Nanoscale Fe_3O_4 from the Single Iron Precursor $FeCl_3$ in Sucroses. In our work, $FeCl_3$ is an inexpensive iron precursor, sucrose is a green and facile sugar, and the preparation procedure does not need purgation or protection with nitrogen or argon; therefore, the results of this investigation are potentially of importance for the industrial large-scale preparation of nanoscale magnetite particles. In this case, magnetite nanoparticles were produced using only the Fe(III) precursor, $FeCl_3$, in a sucrose aqueous solution. As is well-known, the structure of sucrose has no reducing aldehyde, ketone, hemiacetal, or hemiketal groups, and it is a so-called nonreducing sugar that usually cannot reduce Fe^{3+} ions to form Fe_3O_4.[33] A control experiment without the addition of sucrose (Figure 4) was employed to study the function of sucrose. From the TEM and XRD results, only much larger and more polydispersed hematite (α-Fe_2O_3, JCPDS no. 33-0664) particles were obtained when compared with the magnetite particles synthesized in sucrose (see Figures 1 and 2). This means that sucrose perhaps acts as a bifunctional agent: both as the precursor of the reducing agent that partly reduces Fe^{3+} ions to Fe^{2+} ions for the formation of Fe_3O_4 instead of α-Fe_2O_3 and as the source of the coating agent, which leads to the formation of much smaller Fe_3O_4 nanoparticles.

This is unexpected because sucrose is known as a nonreducing sugar, which ordinarily does not reduce Fe^{3+} ions.[33] However, the results that we obtained show that the addition of sucrose to the reaction system is necessary for the formation of Fe_3O_4 from $FeCl_3$. In this situation, Fe^{3+} ions must be partly reduced to Fe^{2+} ions by some intermediate product, most probably a reducing species that comes from sucrose. To confirm this hypothesis, mass spectrometry was used to analyze the difference between the raw sucrose (Figure 5a) and the organic byproducts of the reaction solution that remain after removal of the particles from the synthesis reaction. Because the byproducts obtained by this analysis for all the samples are very similar, only the sample c system (Figure 5b) is discussed here in detail. Figure 5a, obtained with the starting sucrose reactant, shows the only presence of sucrose. Figure 5b, the byproduct

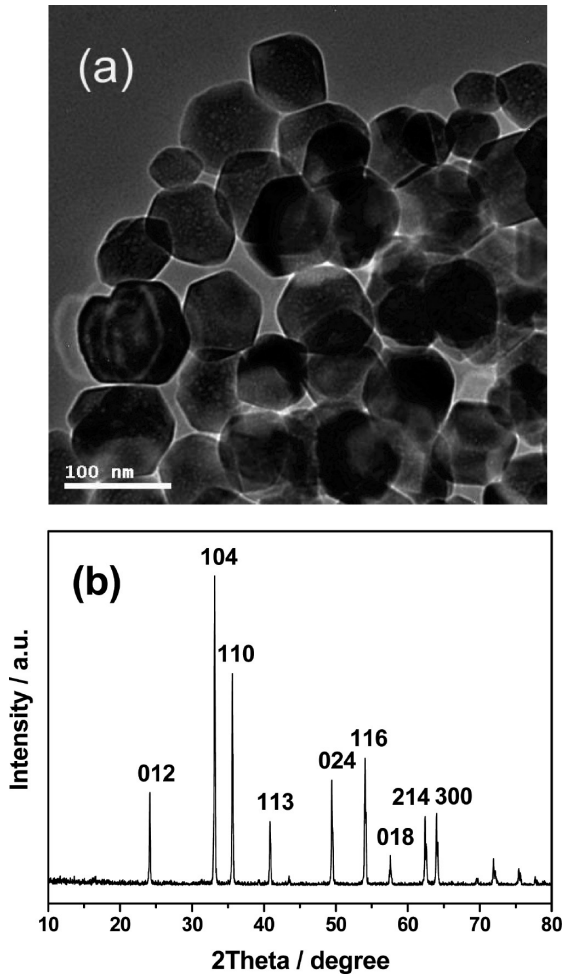

Figure 4. TEM image (a) and XRD pattern (b) of the as-synthesized α-Fe_2O_3 particles without the addition of sucrose.

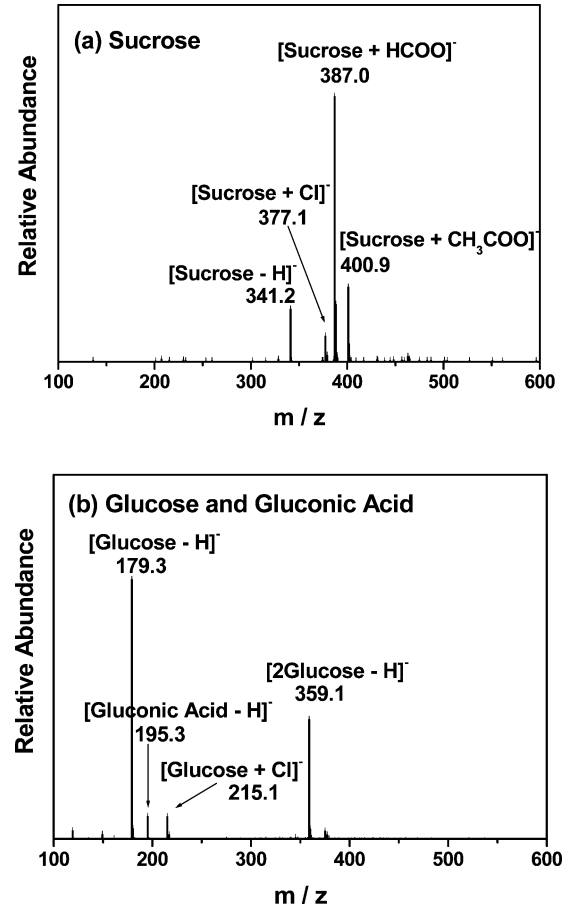

Figure 5. (a) Negative ion mass spectrometry (MS) of raw sucrose. (b) Organic remainders (glucose and gluconic acid) of the reaction solution for sample c after removal of the magnetite particles by centrifugation.

that is present after the reaction, reveals the presence of glucose and gluconic acid (because of the facile epimerization between glucose (MW = 180) and fructose (MW = 180), glucose, here and in Scheme 1, is, in actuality, a mixture of glucose and fructose[33]). The MS results suggest that, during the preparation of magnetite nanoparticles, sucrose decomposes to glucose, a reducing sugar, and that the Fe^{3+} ions are partly reduced by glucose to form Fe_3O_4 and, at the same time, glucose is oxidized to gluconic acid. In accordance with these results and analysis, a possible reduction mechanism leading to the formation of Fe_3O_4 only from the single iron precursor, $FeCl_3$, is proposed in Scheme 1. First, $FeCl_3$ hydrolyzes to form ferric hydroxide and releases H^+ ions, and then sucrose decomposes to produce the reducing sugar, glucose (and fructose), in the proper pH value and temperature. After that, ferric hydroxide is partially reduced by glucose to form Fe_3O_4, while glucose is oxidized to gluconic acid. That is why magnetite (Fe_3O_4) could be synthesized successfully in sucrose (a nonreducing sugar) only from the single iron precursor, ferric chloride ($FeCl_3$).

SCHEME 1: Proposed Reduction Mechanism for the Formation of Fe_3O_4 Only from the Single Iron Precursor, $FeCl_3$, in Sucrose

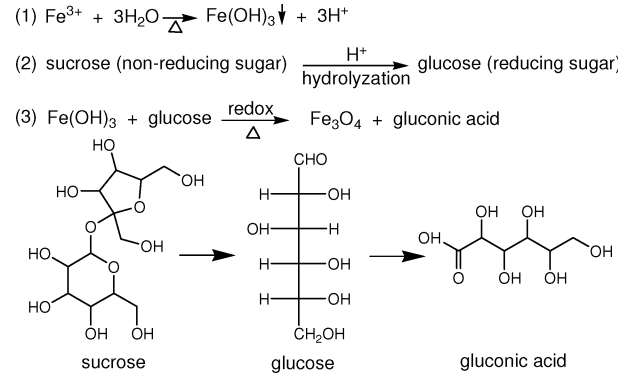

By contrast of the TEM results in Figures 1 and 4, much smaller nanomagnetite particles with uniform particle sizes (from 4 to 16 nm) have been obtained in sucrose solution. However, in the case of the sucrose-free system, only much larger particles with polydispersion (from 53 to 106 nm) could be obtained due to the nucleation and subsequent growth of particles taking place in an uncontrolled manner. It is important to mention that, in the magnetite synthesis system, raw sucrose, glucose (decomposition product of sucrose), and gluconic acid (oxidized product of glucose) are all with multiple hydroxyl groups, especially gluconic acid with carboxy groups; they can adsorb onto certain crystal planes or chelate with the Fe atoms as a coating agent to form steric hindrance, similar to the conventional surfactants and stabilizers.[34] After the formation of magnetite particles, all sucroses transform to glucoses and gluconic acids (see Figure 5b), which coat on the surface of the magnetite nanoparticles, as shown in Figure 6. The complexation leads to the nucleation and subsequent growth of the nanocrystalline in a controlled manner, resulting in an improvement in the uniformity of crystallite morphology and a decrease of the particle size. The

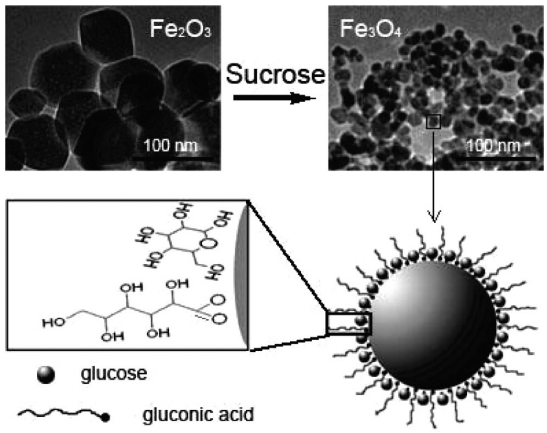

Figure 6. Schematic illustration of coated Fe_3O_4 nanoparticles with glucose and gluconic acid. Note that the structures of the coating agents on the surface of the nanoparticles are simplified.

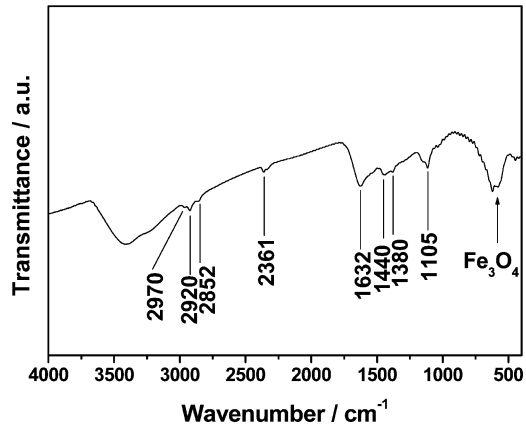

Figure 7. FT-IR spectrum of the as-synthesized magnetite nanoparticle sample c.

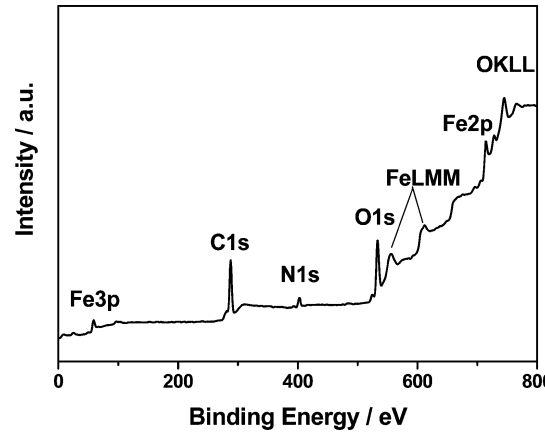

Figure 8. XPS spectrum of the as-synthesized magnetite nanoparticle sample c.

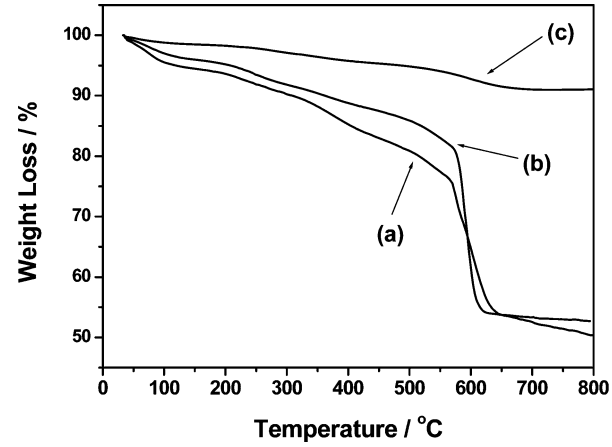

Figure 9. TGA curves of the as-synthesized magnetite nanoparticles with various sucrose concentrations (molar ratio of sucrose to $FeCl_3$ was 7:4 (sample a), 7:8 (sample b), and 7:16 (sample c).

small amount of coating agent, therefore, plays a critical role in modifying the particle and crystalline characteristics.

The presence of the coating agents on the surface of the magnetite nanoparticles was also supported by the FT-IR spectroscopy analysis. Figure 7 shows FT-IR spectroscopy of the as-prepared magnetite sample c. The broad characteristic band from 3600 to 3100 cm^{-1} could be assigned to O−H stretching vibration arising from hydroxyl groups on nanoparticles and adsorbed glucose, gluconic acid, and water.[35] The peaks around 2920 and 2852 cm^{-1}, assignable to asymmetric and symmetric vibrations of C−H in $-CH_2-$, can be obviously found.[36] As we know, two binding modes have been suggested for the surface carboxylate bonding.[37] In one mode, the carboxylate is bound symmetrically to the surface and the symmetrical C═O stretching band should appear at 1404 cm^{-1}.[38] In the other mode, the carboxylate is connected to the surface through one oxygen atom, and the corresponding symmetric C═O (1440 cm^{-1}) stretching was observed in our experiment, which indicated that the carboxylate in this work might bind to the magnetite surface through one oxygen atom.[39] Characteristic bands at 2970 cm^{-1} (asymmetric stretching) and 1380 cm^{-1} (symmetrical deformation vibration) of C−H in $-CH_3$ might arise from the side reaction products of sucrose during the hydrothermal reaction. The band at 1105 cm^{-1} of C−O−C stretching almost came from the residue sucrose. In addition, the absorption band at 1632 and 2361 cm^{-1} on the spectrum referred to the vibration of the remainder H_2O and adsorbed CO_2, respectively, in the sample.[35,40] A strong absorption band at 579 cm^{-1} is related to the vibrations of the Fe−O functional group, which corroborates that the phase of as-prepared particles is magnetite.[41] The absorption band at 618 cm^{-1} might be assigned to the existence of some amount of oxidized maghemite on the magnetite surface. Figure 8 shows the XPS spectrum of the coated magnetite nanoparticle sample c. The appearance of the characteristic peaks of Fe 2p and O 1s is typical for iron oxide, whereas the peaks ascribed to C 1s and O1s at expected positions further indicate the existence of a glucose and gluconic acid coating on the surface of the magnetite nanoparticles.[42] The peak ascribed to N 1s may come from amide, which was obtained from the reaction of gluconic acid and $NH_3 \cdot H_2O$.[33]

The formation of uniform magnetite nanoparticles can be attributed to the attachment of the coating agents on the particle surface. The existence of coating agents prevents the coalescence of particles due to the steric hindrance between the coating agents. Thus, the sucrose concentration plays an important role in the preparation of uniform and size-controlled nanoparticles. TGA measurement can identify the coating agents on the surface of the magnetite nanoparticles at different percentages. As demonstrated in Figure 9, TGA analysis of samples a, b, and c was performed under nitrogen atmosphere to minimize the mass increase due to Fe^{2+} ions' oxidation and only allow the coating agents to decompose thermally. All the TGA curves display two weight loss processes. The first weight loss should be attributed to the dehydration of the samples, and the second weight loss corresponds to the desorption and subsequent evaporation of the coating agents, including glucose and glu-

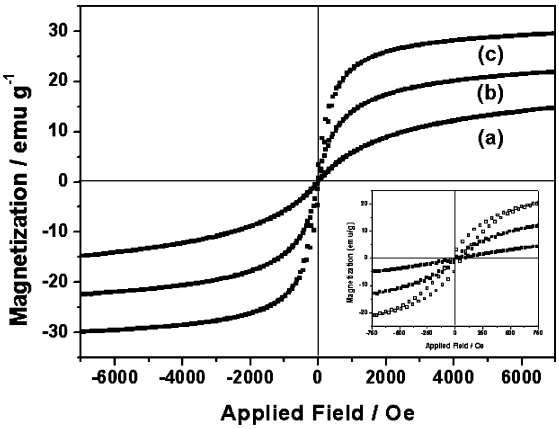

Figure 10. Magnetization curves at room temperature of magnetite samples a, b, and c (molar ratio of sucrose to $FeCl_3$ was 7:4 (sample a), 7:8 (sample b), and 7:16 (sample c).

conic acid. By contrast, the larger the sucrose concentration is, the higher the percentage of weight loss is, which corresponds to the smaller particle size (see Table 1) and indicates that the higher sucrose concentration favors the formation of smaller nanoparticles.

All of the above data strongly indicate that there are interactions between Fe_3O_4 nanoparticles and glucose and gluconic acid. The distinct coating amount of surfactants will make a dissimilar effect on the nucleation and growth of particles, so the size and morphology of the magnetite nanoparticles could be controlled in this way. The particles with smaller size have a larger surface area that can adsorb a larger amount of coating agents on the particle surface, and vice versa. Furthermore, in view of the strong coordination ability of the hydroxyl and carboxy groups of the coating agents and the rapid hydrolysis of Fe^{3+}, the nucleation rate of the Fe species should be very high,[43] leading to the formation of ultrathin and homogeneous crystal nuclei in the composites of the glucose and gluconic acid system. On the other hand, these composites act as the coating agents of the Fe species and greatly suppress the growth and aggregation of Fe nuclei due to steric hindrance, following a decrease in the crystallization rate of magnetite. With the increasing of the sucrose concentration, the rate of nucleation increases and the steric hindrance effect becomes larger, which lead to the decreasing of particles size. As a result, the rapid nucleation and the slow crystallization of magnetite were obtained in the presence of sucrose, which led to the formation of uniform magnetite nanoparticles, and the particle size could be controlled easily by adjusting the sucrose concentration.

Magnetic Measurements. Magnetization curves of all the samples measured at room temperature are shown in Figure 10. Samples a, b, and c show almost immeasurable coercivity and remanence, suggesting that these nanoparticles are superparamagnetic at room temperature.[44] The saturation magnetization (*M*s) of all the samples increases from 14.82 to 21.95 to 29.55 emu g^{-1} at 7 KOe with decreasing sucrose concentration, which can be attributed to the growth of particle size, enhancement in crystallinity, and reduction of surface adsorbed species.[45] The decrease of the saturation magnetization of all the samples than the bulk magnetite (92 emu g^{-1})[46] is often observed with the nanoparticles and is most likely attributed to the existence of organic coating agents.[45] Some studies suggested that the presence of the coating agents decreases the uniformity due to quenching of surface moments, resulting in the reduction of magnetic moment in such nanoparticles.[47] Sample c with a hysteresis loop exhibits a low magnetic coercivity of 46.68 Oe, which may be because, for sample c, the size of some particles exceeds the superferromagnetic critical size.

Conclusions

A simple and facile hydrothermal reduction route has been employed to synthesize the coated magnetite nanoparticles with glucose and gluconic acid only from the cheap Fe(III) precursor, $FeCl_3$, in sucrose. The particle size of the as-synthesized magnetite could be easily controlled from 4 to 16 nm by changing the feeding concentration of sucrose. The effective mechanism of sucrose was discussed in detail. Sucrose functions as a bifunctional agent: both as the precursor of the reducing agent to make the formation of the magnetite phase only from the Fe(III) precursor, $FeCl_3$, and as the source of the coating agent to prevent particle growth and agglomeration by chelating with metal ions. We believe that these coated magnetite nanoparticles will have promising applications not only in biotechnology and biomedicine but also in magnetic resonance imaging and catalysis. In addition, because the purgation or protection procedure is not necessary, this simple approach allows the synthesis of magnetite nanoparticles to be extended into the industrial range with mass production. All the as-synthesized magnetite nanoparticles are superparamagnetic, and the saturation magnetization (*M*s) is greatly related to the particle size.

Acknowledgment. This research was financially supported by the National Basic Research Program of China (also called 973, Grant No. 2009CB623502), the National Natural Science Foundation of China (Grant Nos. 20573059 and 20777039), the International S&T Cooperation Program of China (Grant No. 2007DFA90720), the Doctoral Program Foundation of the Ministry of Education, China (Grant No. 20070055012), and the Fok Ying Tung Education Foundation (Grant No. 114039). Our deepest gratitude goes to Dr. Yifeng Shi and Mr. Yichi Zhang for their help in valuable discussions and writing.

Supporting Information Available: High-magnification TEM images. This material is available free of charge via the Internet at http://pubs.acs.org.

References and Notes

(1) Billas, I. M. L.; Chatelain, A.; de Heer, W. A. *Science* **1994**, *265*, 1682.
(2) Ashoori, R. C. *Nature* **1996**, *379*, 413.
(3) Hu, A. G.; Yee, G. T.; Lin, W. B. *J. Am. Chem. Soc.* **2005**, *127*, 12486.
(4) Raj, K.; Moskowitz, R. *J. Magn. Magn. Mater.* **1990**, *85*, 233.
(5) Arico, A. S.; Bruce, P.; Scrosati, B.; Tarascon, J. M.; Schalkwijk, W. V. *Nat. Mater.* **2005**, *4*, 366.
(6) Lee, H.; Lee, E.; Kim, D. K.; Jang, N. K.; Jeong, Y. Y.; Jon, S. Y. *J. Am. Chem. Soc.* **2006**, *128*, 7383.
(7) Wang, P.; Shi, Q. H.; Liang, H. J.; Steuerman, D. W.; Stucky, G. D.; Keller, A. A. *Small* **2008**, *4*, 2166.
(8) Wang, P.; Shi, Q. H.; Shi, Y. F.; Clark, K. K.; Stucky, G. D.; Keller, A. A. *J. Am. Chem. Soc.* **2009**, *131*, 182.
(9) Roullin, V. G.; Deverre, J. R.; Lemaire, L.; Hindre, F.; Julienne, M. C. V.; Vienet, R.; Benoit, J. P. *Eur. J. Pharm. Biopharm.* **2002**, *53*, 293.
(10) Kim, D. K.; Zhang, Y.; Kehr, J.; Klason, T.; Bjelke, B.; Muhammed, M. *J. Magn. Magn. Mater.* **2001**, *225*, 256.
(11) Lu, A. H.; Salabas, E. L.; Schüth, F. *Angew. Chem., Int. Ed.* **2007**, *46*, 1222.
(12) Jeong, U.; Teng, X. W.; Wang, Y.; Yang, H.; Xia, Y. N. *Adv. Mater.* **2007**, *19*, 33.
(13) Kang, Y. S.; Risbud, S.; Rabolt, J. F.; Stroeve, P. *Chem. Mater.* **1996**, *8*, 2209.
(14) Zhou, Z. H.; Wang, J.; Liu, X.; Chan, H. S. O. *J. Mater. Chem.* **2001**, *11*, 1704.

(15) Wang, X.; Zhuang, J.; Peng, Q.; Li, Y. D. *Nature* **2005**, *437*, 121.
(16) Kumar, R. V.; Koltypin, Y.; Xu, X. N.; Yeshurun, Y.; Gedanken, A.; Felner, I. *J. Appl. Phys.* **2001**, *89*, 6324.
(17) Pinna, N.; Garnweitner, G.; Antonietti, M.; Niederberger, M. *J. Am. Chem. Soc.* **2005**, *127*, 5608.
(18) Rockenberger, J.; Scher, E. C.; Alivisatos, P. A. *J. Am. Chem. Soc.* **1999**, *121*, 11595.
(19) Hyeon, T.; Lee, S. S.; Park, J.; Chung, Y.; Na, H. B. *J. Am. Chem. Soc.* **2001**, *123*, 12798.
(20) Sun, S. H.; Zeng, H.; Robinson, D. B.; Raoux, S.; Rice, P. M.; Wang, S. X.; Li, G. X. *J. Am. Chem. Soc.* **2004**, *126*, 273.
(21) Dunin-Borkowski, R. E.; McCartney, M. R.; Frankel, R. B.; Bazylinski, D. A.; Posfai, M.; Buseck, P. R. *Science* **1998**, *282*, 1868.
(22) Park, J.; Lee, E.; Hwang, N. M.; Kang, M. S.; Kim, S. C.; Hwang, Y.; Park, J. G.; Noh, H. J.; Kini, J. Y.; Park, J. H.; Hyeon, T. *Angew. Chem., Int. Ed.* **2005**, *44*, 2872.
(23) Kotal, S. A.; Mandal, T. K.; Giri, S.; Nakamura, H.; Kohara, T. *Chem. Mater.* **2004**, *16*, 3489.
(24) Yu, W. W.; Falkner, J. C.; Yavuz, C. T.; Colvin, V. L. *Chem. Commun.* **2004**, *20*, 2306.
(25) Lalatonne, Y.; Richardi, J.; Pileni, M. P. *Nat. Mater.* **2004**, *3*, 121.
(26) Kim, M.; Chen, Y. F.; Liu, Y. C.; Peng, X. G. *Adv. Mater.* **2005**, *17*, 1429.
(27) Wang, L. Y.; Bao, J.; Wang, L.; Zhang, F.; Li, Y. D. *Chem.—Eur. J.* **2006**, *12*, 6341.
(28) Ge, J. P.; Hu, Y. X.; biasini, M.; Dong, C. L.; Guo, J. H.; Beyermann, W. P.; Yin, Y. D. *Chem.—Eur. J.* **2007**, *13*, 7153.
(29) Molday, R. S.; Mackenzie, D. *J. Immunol. Methods* **1982**, *52*, 353.
(30) Daou, T. J.; Pourroy, G.; Begin-Colin, S.; Greneche, J. M.; Ulhaq-Bouillet, C.; Legare, P.; Bernhardt, P.; Leuvrey, C.; Rogez, G. *Chem. Mater.* **2006**, *18*, 4399.
(31) Pinna, N.; Grancharov, S.; Beato, P.; Bonville, P.; Antonietti, M.; Niederberger, M. *Chem. Mater.* **2005**, *17*, 3044.
(32) Bersani, D.; Lottici, P. P.; Montenero, A. *J. Raman Spectrosc.* **1999**, *30*, 355.
(33) Wade, L. G., Jr. *Organic Chemistry*; Prentice Hall/Pearson Education: Upper Saddle River, New Jersey, 2003.
(34) Cushing, B. L.; Kolesnichenko, V. L.; O'Connor, C. J. *Chem. Rev.* **2004**, *104*, 3893.
(35) Cai, W.; Wan, J. Q. *J. Colloid Interface Sci.* **2007**, *305*, 366.
(36) Liang, X.; Wang, X.; Zhuang, J.; Chen, Y. T.; Wang, D. S.; Li, Y. D. *Adv. Funct. Mater.* **2006**, *16*, 1805.
(37) Tao, Y. T. *J. Am. Chem. Soc.* **1993**, *115*, 4350.
(38) Harris, L. A.; Goff, J. D.; Carmichael, A. Y.; Riffle, J. S.; Harburn, J. J.; St. Pierre, T. G.; Saunders, M. *Chem. Mater.* **2003**, *15*, 1367.
(39) Shafi, K. V. P. M.; Ulman, A.; Yan, X. Z.; Yang, N.; Estournes, C.; White, H.; Rafailovich, M. *Langmuir* **2001**, *17*, 5093.
(40) Rajh, T.; Chen, L. X.; Lukas, K.; Liu, T.; Thurnauer, M. C.; Tiede, D. M. *J. Phys. Chem. B* **2002**, *106*, 10543.
(41) Cornell, R. M.; Schwertmann, U. *The Iron Oxides*; Wiley-VCH: Weinheim, Germany, 1996.
(42) Lu, X. F.; Yu, Y. H.; Chen, L.; Mao, H. P.; Gao, H.; Wang, J.; Zhang, W. J.; Wei, Y. *Nanotechnology* **2005**, *16*, 1660.
(43) Li, L. D.; Sun, X. H.; Yang, Y. L.; Guan, N. J.; Zhang, F. X. *Chem.—Asian J.* **2006**, *1*, 664.
(44) Li, Z.; Sun, Q.; Gao, M. Y. *Angew. Chem., Int. Ed.* **2005**, *44*, 123.
(45) Goya, G. F.; Berquo, T. S.; Fonseca, F. C.; Morales, M. P. *J. Appl. Phys.* **2003**, *94*, 3520.
(46) Han, D. H.; Wang, H. L.; Luo, J. *J. Magn. Magn. Mater.* **1994**, *136*, 176.
(47) Kim, D. K.; Mikhaylova, M.; Zhang, Y.; Muhammed, M. *Chem. Mater.* **2003**, *15*, 1617.

JP9038682